First-principles study of filled and unfilled antimony skutterudites

2007 J. Phys.: Condens. Matter 19 096002

(http://iopscience.iop.org/0953-8984/19/9/096002)

IOP PUBLISHING JOURNAL OF PHYSICS: CONDENSED MATTER

J. Phys.: Condens. Matter **19** (2007) 096002 (19pp) doi:10.1088/0953-8984/19/9/096002

First-principles study of filled and unfilled antimony skutterudites

Philippe Ghosez and Marek Veithen

Département de Physique, Université de Liège, B-5, B-4000 Sart-Tilman, Belgium

Received 19 July 2006, in final form 8 December 2006
Published 12 February 2007
Online at stacks.iop.org/JPhysCM/19/096002

Abstract

Using a first-principles approach based on density-functional theory, the electronic, dielectric and dynamical properties of the skutterudites $CoSb_3$ and $TlFeCo_3Sb_{12}$ are studied. In particular, the electron localization tensor, static and dynamic effective charges, static and optical dielectric constants and phonon dispersion curves are computed. The Born effective charges are found to be significantly larger than the static charges of the ions. Moreover, the static dielectric constant of $TlFeCo_3Sb_{12}$ is found to be significantly larger than that of $CoSb_3$. The analysis of the phonon dispersion curves reveals a low-energy mode due to coupled vibrations of Tl and Sb. This mode is at the origin of a well-defined peak in the phonon density of states of $TlFeCo_3Sb_{12}$ and its mode effective charge is related to the increase of the dielectric constant in $TlFeCo_3Sb_{12}$. Our results are compared to recent experiments performed on $CoSb_3$ and $TlFeCo_3Sb_{12}$, and differences between the lattice dynamics of $TlFeCo_3Sb_{12}$ and other filled skutterudites are highlighted.

1. Introduction

$CoSb_3$ belongs to the class of binary skutterudites [1] which are characterized by a complex crystalline structure containing large voids and four formula units per cell. It has been observed that filling the voids with electropositive atoms such as Tl or rare earth atoms leads to a drastic decrease of the lattice thermal conductivity [2, 3]. Combined with good electronic properties (electrical conductivity, Seebeck coefficient), this makes the so-called filled skutterudites potentially interesting for thermoelectric applications such as refrigeration or energy generation [4].

One mechanism that has been evoked to explain the strong reduction of the lattice thermal conductivity in filled skutterudites is a strongly anharmonic rattling motion of the filling atom. Keppens and co-workers [5] used inelastic neutron scattering to measure the phonon density of states (DOS) of La in $LaFe_4Sb_{12}$. They found a well-defined peak at about 56 cm^{-1} and a somewhat broader structure around 121 cm^{-1} that were associated to two La-dominated localized modes. Feldman and co-workers [6] used a force constant model fitted from first-principles calculations to compute the phonon dispersion relations and DOS of $LaFe_4Sb_{12}$ and

$CeFe_4Sb_{12}$. Their results allowed them (i) to refute the hypothesis of an anharmonic rare earth potential and (ii) to suggest that the second peak in the La-projected DOS is not related to a true localized mode. It is instead the result of hybridizations between the rare earth and Sb vibrations.

In several respects, we can expect the behaviour of Tl to be different from that of La and Ce. First, the 4f valence states of the rare earth atoms strongly hybridize with the transition metal d and Sb p states in the vicinity of the Fermi energy [8]. These hybridizations are absent in the case of Tl where the 4f states are much lower in energy. Second, the electronegativity of Tl is significantly higher than that of La and Ce and close to that of Sb. This suggests that Tl may have a smaller effect on the electrical transport properties of $CoSb_3$ than the rare earths. Finally, the ionic radius of Tl is significantly larger than that of La or Ce. We can therefore expect the dynamical properties of Tl to be significantly different from that of the rare earths.

Some evidence of a different behaviour of Tl can be found in a recent work of Hermann and co-workers [9], who measured the phonon DOS of various Tl-filled skutterudites. These authors found a single peak around 40 cm^{-1}, in striking difference with the two peaks of the La-filled compound.

In this work, we use a first-principles density-functional approach to study the dielectric and dynamical properties of $CoSb_3$ and of a model crystal of $TlFeCo_3Sb_{12}$, where we neglect any configurational disorder due to Fe. Up to now, first-principles studies performed on skutterudites were restricted to Ce and La filling and concerned their electronic and dynamical properties [6–8, 26, 28, 29]. No theoretical calculations either investigated the dielectric constants or Born effective charges, or focused on Tl filling. The aim of this work is (i) to give a theoretical interpretation of the results of [9] in order to clarify the distinct dynamical properties of Tl- and La-filled skutterudites, and (ii) to provide accurate theoretical data on the dielectric properties of skutterudites. We show that Tl is in a harmonic potential up to large displacements. Moreover, the peak about 40 cm^{-1} in the Tl-projected DOS is due to the vibrational motion of Tl that shows only modest hybridizations with the normal modes of the host crystal. These hybridizations are more important in $LaFe_4Sb_{12}$, where they give rise to a second peak in the La-projected DOS. The Born effective charges and the dielectric constants are found to be large in $CoSb_3$ and $TlFeCo_3Sb_{12}$. In addition, the electronic and static dielectric constants are significantly larger in the filled compound than in the unfilled compound. The mechanisms responsible for this behaviour are general, and might be used to tune the dielectric properties of other compounds.

Our paper is organized as follows. In section 2, we describe the theoretical framework of our calculations. In section 3, we discuss the structural and electronic properties of $CoSb_3$ and $TlFeCo_3Sb_{12}$. In section 4, we report their optical dielectric constant and effective charges. In section 5, we focus on the zone-centre phonons in the filled and unfilled compounds and deduce their static dielectric tensor and infrared reflectivity. Finally, in section 6, we compare the phonon dispersion curves of $CoSb_3$ and $TlFeCo_3Sb_{12}$.

2. Technical details

Our calculations were performed within the local-density approximation to density-functional theory (DFT) [10, 11] using the ABINIT [12] package. For the purpose of reporting theoretical phonon frequencies more directly comparable to experimental data, we worked at the experimental lattice constant. The atomic positions were relaxed until the forces on the atoms were smaller than 2.5×10^{-3} eV $Å^{-1}$. For the exchange–correlation energy, we used the parameterization of Perdew and Wang [13]. The valence states were computed non-relativistically. The all-electron potentials were replaced by norm-conserving pseudopotentials

Table 1. Parameters used to generate the pseudopotentials of Fe, Co, Sb and Tl. Reported is the type of the pseudopotential (H = Hamann, TM = Troullier–Martins), the projector that is used as the local component, the cutoff radii (bohr) of the s, p, d and f channels (in case they have been included in the pseudopotential) and the cutoff radius (bohr) of the partial core density (r_{nlc}). The values in brackets indicate the reference energy (eV) that has been used to build the pseudo-wavefunction in case we did not use the default value of the FHI98PP code.

	Fe	Co	Sb	Tl
Type	H	H	TM	H
Configuration	$4s^1 3d^6 4p^0$	$4s^1 3d^7 4p^0$	$5s^2 5p^3$	$6s^2 5d^{10} 6p^0$
Local part	f	f	s	p
s channel	1.2	1.2	1.8	1.4
p channel	1.2 (5.0)	1.2 (5.0)	2.0	1.4
d channel	1.0	1.0	2.5 (15.0)	1.4
f channel	1.6[a]	1.6[a]	—	1.6[a]
r_{nlc}	0.9	0.9	1.5	1.0

[a] Default value used by the FHI98PP code.

generated from scalar relativistic all-electron calculations of the free atoms using the FHI98PP code [14]. The Sb potential was generated according to the Troullier–Martins scheme [15]. Hamann [16] pseudopotentials were chosen for Co, Fe and Tl. The parameters used to generate the pseudopotentials are summarized in table 1. The electronic wavefunctions were expanded in a plane wave basis. With the pseudopotentials described above a kinetic energy cutoff of 25 Hartree was enough to obtain well-converged results.

A $2 \times 2 \times 2$ grid of special k-points [19] was sufficient to obtain well-converged phonon frequencies, while a $4 \times 4 \times 4$ grid was required for the Born effective charges, dielectric tensors and localization tensors. For the $2 \times 2 \times 2$ grid, the violation of the charge neutrality for the Born effective charges [20] was quite important ($0.2|e|$, where $|e|$ is the charge of a proton). Using the $4 \times 4 \times 4$ grid, this error was reduced by a factor of 10, while the phonon frequencies changed by less than 3 cm^{-1}.

The static ionic charges of section 4.2 were computed following Bader's prescription for the partitioning of space into atomic basins [17], as is described in [18].

The phonon frequencies, Born effective charges, localization tensors and dielectric tensors were computed from a linear response approach to DFT [20–22]. The first-order derivatives of the wavefunctions were calculated by minimizing a variational expression of the second-order energy derivatives within the parallel gauge. In order to perform the band-by-band decomposition of various quantities such as the localization tensor or the optical dielectric tensor, these wavefunctions were further transformed to the diagonal gauge [23]. We computed the dynamical matrix explicitly on a $2 \times 2 \times 2$ grid of special q-points. To obtain the full phonon band structure and DOS, we used a Fourier interpolation that includes the long-range dipole–dipole interactions [24]. The lattice specific heat was computed from the DOS as is described in [25]. This approach is more accurate than the one used in the previous studies of Singh and co-workers [6, 7, 26]. In [6] and [26], these authors used an empirical force constant model that had been fitted on LDA total energy calculations, while in [7] they computed the interatomic force constants for zone-centre atomic displacements only.

3. Ground-state properties

3.1. Crystal structure

The structure of $CoSb_3$ is formed of a bcc lattice (space group $Im\bar{3}$, lattice constant a = 9.0385 Å) with four formula units per primitive (rhombohedral) cell. It can be described as a

distorted perovskite [1] with the chemical formula ABO_3. In $CoSb_3$, the site of the A atoms is empty, the sites of the B atoms are occupied by Co and the sites of O by Sb. The $CoSb_6$ octahedra are tilted so that the Sb atoms form rectangular Sb_4 rings. The Co and Sb atoms occupy respectively the 8c $(\frac{1}{4}, \frac{1}{4}, \frac{1}{4})$ and 24g $(0, y, z)$ Wyckoff positions. The relaxed values of the reduced coordinates $y = 0.332\,84$ and $z = 0.159\,65$ are in excellent agreement with the experimental results [27] of $y = 0.335\,37$ and $z = 0.157\,88$.

In the unfilled compound, the 2a $(0, 0, 0)$ Wyckoff positions are unoccupied. They are the centres of large voids surrounded by 12 Sb and 8 Co atoms. These voids are able to accommodate an electropositive filler such as Tl or various rare earth atoms. The electronic configuration of Tl is $6s^2 6p^1$. In order to fill an important fraction of voids, x, all chemical bonds must be saturated. Therefore, one has to compensate the excess charge due to the Tl 6p electrons by replacing for example one Co per cell by Fe or one Sb by Sn [3].

Experimentally, the lattice constant of Tl-filled $CoSb_3$ is found to increase linearly with the amount of filled voids [3] for $0 < x < 0.8$. In our calculation, we worked at $x = 1$ and we replaced one Co per cell by Fe. We chose a lattice constant of 9.1276 Å that corresponds to a linear extrapolation of the data of [3] to $x = 1$. This choice is further justified by the fact that the residual stress in the filled compound (0.049 eV $Å^{-3}$) is similar to the stress in the unfilled compound (0.046 eV $Å^{-3}$). The relaxed reduced atomic coordinates in $TlFeCo_3Sb_{12}$ and $CoSb_3$ differ by less than 0.003.

Our calculations were performed applying periodic boundary conditions to the rhombohedral unit cells of $CoSb_3$ and $TlFeCo_3Sb_{12}$ that contain half the atoms of the corresponding bcc unit cells. In the case of $TlFeCo_3Sb_{12}$, the Fe atoms therefore occupy the same crystallographic site in each cell. This situation is somewhat artificial, since it neglects any configurational disorder introduced by the random substitution of Co by Fe in real samples. However, it constitutes a first step towards the understanding of $TlFeCo_3Sb_{12}$. Further improved treatment of the disorder would require much more refined (and computationally very demanding) approaches and is out of the scope of the present paper. We expect the lack of disorder in our calculations to have only modest effects on the electronic and dynamical properties of Tl for the Fe-compensated compound, while it might be more important for other compensations such as the substitution of Sb by Sn. First, Fe can only occupy four equivalent sites per rhombohedral cell, while Sn can occupy 12 sites. Second, the distances between Tl and Sb (3.3897 and 3.3977 Å) are smaller than the distance between Tl and Co (3.9823 Å). Finally, we will see in section 6 that the vibrations of Co/Fe are strongly decoupled from the vibrations of Tl and located in the high-energy region above 200 cm^{-1} of the phonon spectrum. In contrast, the vibrations of Sb occupy the region below 200 cm^{-1} and show significant hybridizations with the vibrations of Tl.

3.2. Electronic properties

The left part of figure 1 shows the LDA band structure of $CoSb_3$ between the high-symmetry points N, Γ, and P. The top of the valence bands was fixed to 0 eV. There is a good agreement between our results and the band structures obtained in previous studies [28–31]. We observe the presence of two well-separated groups of valence bands. The bands between −13 and −7 eV are mainly composed of Sb 5s states while the valence bands above −6 eV result from hybridizations between Sb 5p and Co 3d states.

There is some controversy about the energy of the band gap, E_g, in $CoSb_3$. Experimentally, values between 0.03 and 0.7 eV have been reported (see [32–34] and references therein). From a theoretical point of view, there is a similar broad set of values in the literature. The band gap is defined by a highly dispersive band at the Γ-point. We obtain a value of 0.24 eV, in

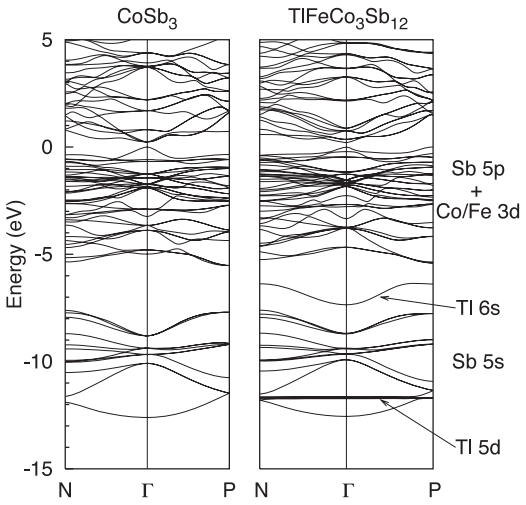

Figure 1. Electronic band structure in $CoSb_3$ and $TlFeCo_3Sb_{12}$.

reasonable agreement with other first-principles LDA and GGA calculations (0.05 eV [29], 0.22 eV [28], 0.195 and 0.330 eV [30], 0.140 eV [31]). This discrepancy between the theoretical results has been attributed to a strong dependence of E_g on the position of the Sb atoms together with the well-known problem of the LDA and GGA to predict the correct band gap of semiconductors [28, 30].

In $TlFeCo_3Sb_{12}$, (right part of figure 1), the band gap (0.20 eV) is slightly smaller than in the unfilled compound. In addition, we observe two additional groups of bands that are related to the atomic orbitals of Tl. The Tl 5d states form a flat set of bands that are in the same energy region as the Sb 5s states. Due to the lack of dispersion, these states can be considered as inert. In contrast, the Tl 6s states form a band at about -7 eV that shows a significant dispersion related to a covalent interaction with the electronic states of the host crystal. This point will be investigated in more detail below.

In some cases, the filling of the voids in skutterudites does not only affect the lattice thermal conductivity but also the electronic transport properties. For example, the Ce 4f states in $CeFe_4Sb_{12}$ hybridize with the Fe 3d and Sb 5p states to form a set of flat conduction bands in the vicinity of the Fermi level [8]. Due to the low dispersion of these bands, the electron effective mass in this compound is quite high, implying a low electron mobility [35]. As can be seen in the right part of figure 1, the effect of Tl on the electronic band structure of $CoSb_3$ is less important. The only additional bands are well below the Fermi level and should therefore not affect the electronic transport properties. To conclude definitively about this point, it might be important to perform a more intensive study of the electronic band structure of $TlFeCo_3Sb_{12}$ that eventually takes into account spin–orbit coupling and alloying effects (see section 3.1).

In order to get additional information on the electronic properties of $CoSb_3$ and $TlFeCo_3Sb_{12}$, we computed the localization tensor (see [36] and references therein) and the electronic density for selected states in these compounds. As we have shown in a previous work [22], the decomposition of the localization tensor into contributions of individual groups of bands can act as a sensitive probe to study hybridizations within a solid. For example, a state that has the same variance in a solid and in the isolated atom can be considered as chemically inert. In contrast, a modification of the variance is usually attributed to covalent interactions of the corresponding orbitals.

Table 2. Variances $\langle r^2 \rangle_c$ (bohr^2) of the groups of bands in $CoSb_3$ and $TlFeCo_3Sb_{12}$ and of the Sb 5s, Tl 5d and Tl 6s electrons calculated on an isolated Sb atom and Tl^+ ion.

Bands	$CoSb_3$	$TlFeCo_3Sb_{12}$	Atom
Sb 5s (+ Tl 5d)	3.06	2.63	1.86[a], 0.85[b]
Tl 6s	—	18.06	2.14
Sb 5p + Co 3d	5.11	5.85	—
E_g (eV)	0.24	0.20	—

[a] Sb 5s orbital of an isolated Sb atom.
[b] Tl 5d orbitals of an isolated Tl^+ ion.

In $CoSb_3$ and $TlFeCo_3Sb_{12}$, the localization tensor is isotropic. In table 2, we report the variances of the two (respectively three) groups of bands defined in section 3.2 as well as the variances of the atomic orbitals Sb 5s, Tl 5d and Tl 6s. In the case of Tl, we used linear response calculations to obtain the variance of the 6s state of an isolated Tl^+ ion. We adopted this configuration because it is close to the configuration we expect for Tl in $TlFeCo_3Sb_{12}$. Moreover, we avoided some problems related to the linear response calculation of the localization tensor for partially occupied states. To use the same approach for Sb, we had to chose Sb^{3+} as the reference configuration. For the 5s state, we obtained a value of 1.51 bohr^2. Unfortunately, the bonding is covalent rather than ionic in $CoSb_3$, and the Sb^{3+} configuration seems therefore somewhat artificial. To determine the variance for the neutral Sb atom, we used the FHI98PP [14] code: we computed the all-electron wavefunction of the 5s state and its variance as a matrix element of the squared position operator x^2.

In $CoSb_3$, the variance of the Sb 5s bands is larger than the variance of the corresponding atomic orbital. This result confirms the participation of these electrons in the Sb–Sb bonding observed previously [30]. In the filled compound, the Tl 5d states occupy the same energy region as the Sb 5s states. Therefore, the formalism of [22] cannot be applied to study the localization of these bands individually. Nevertheless, we can obtain some information on the modification of the Sb 5s states in $TlFeCo_3Sb_{12}$. Due to the flat dispersion of the Tl 5d bands observed in figure 1, it is reasonable to assume that their variance in the solid is close to the value in the isolated Tl^+ ion. If we neglect the covariance between Sb 5s and Tl 5d bands, we obtain a value of 3.37 bohr^2 for the variance of the Sb 5s bands in $TlFeCo_3Sb_{12}$. This result suggests that the Sb 5s electrons are more delocalized in the filled than in the unfilled compound[1].

A stronger variation is found for the variance of the highest occupied bands (Sb 5p + Co 3d). In $TlFeCo_3Sb_{12}$, these electrons are more delocalized than in $CoSb_3$.

The most spectacular evolution concerns the variance of the Tl 6s state. In the solid, this quantity is about nine times larger than in the isolated ion. This result suggests a significant interaction between the Tl 6s orbitals and the electronic states of the host crystal. To get more insight into these hybridizations we plotted the electronic pseudo-density associated with the Tl 6s band. It can be seen in figure 2 that these electrons are partly delocalized on the Sb atoms of the cage, in agreement with a significant covalent interaction between Tl and Sb. Such an interaction is coherent with the fact that Tl can be inserted into the voids of the host crystal in spite of the fact that the crystal radius of Tl^+ in a 12-coordinate site [49] (1.84 Å) is larger than that of the rare earth fillers Ce^{3+} (1.48 Å [58]) and La^{3+} (1.50 Å) and is close to the radius of the cage (about 1.892 Å [37]).

[1] This result remains true even if the covariance between Sb 5s and Tl 5d bands is not zero. As is shown in [22], this quantity is necessarily negative. The variance of the Sb 5s bands will therefore increase even more in case of a non-zero covariance.

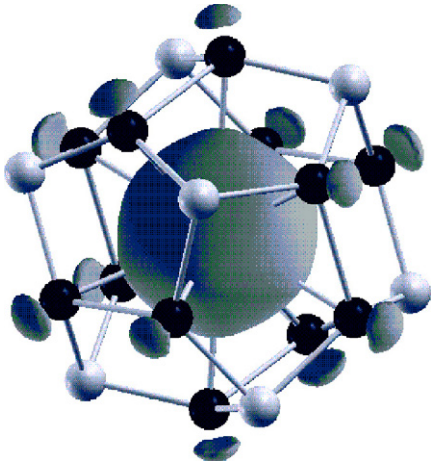

Figure 2. Electronic pseudo-density of the Tl 6s band in $TlFeCo_3Sb_{12}$. The isodensity value corresponds to 10% of the maximum density of this state (0.0088 electron/bohr^3). Tl (not shown) occupies the centre of the cage. The black and grey spheres represent respectively Sb and Co/Fe. This figure has been realized thanks to the XCrySDen [38] crystalline and molecular structure visualization program.

(This figure is in colour only in the electronic version)

In summary, the electronic band structures of $CoSb_3$ and $TlFeCo_3Sb_{12}$ differ in the region well below the Fermi level. On the one hand, the Tl 5d states show a flat dispersion suggesting that these states are chemically inert. On the other hand, the Tl 6s states show a significant dispersion related to a partial delocalization of the corresponding electrons on the Sb atoms of the cage. These hybridizations are expected to affect the dielectric and dynamic properties of Tl in the filled compound.

4. Dielectric properties

4.1. Optical dielectric tensor

In $CoSb_3$, the dielectric tensor is isotropic. The theoretical value $\varepsilon_\infty = 31.67$ is large. Similar large dielectric constants to those in $CoSb_3$ have been computed for other narrow band gap semiconductors such as Al_2Ru (principal values: 18.9, 22.9, 20.7) [41]. Moreover, they have been measured in the skutterudites $CoAs_3$ (26.25) [42], UFe_4P_{12} (17) and $CeFe_4P_{12}$ (31) [43]. The theoretical value of ε_∞ in $CoSb_3$ overestimates the experimental result [39] of 25.6 by about 20%, as is typical in LDA calculations [40].

In the filled compound, the dielectric tensor is no longer isotropic but has weak off-diagonal elements. These elements are about four orders of magnitude smaller than the diagonal ones, and we will not consider them in the discussion that follows. We obtain a value of 38.57 for the dielectric constant in $TlFeCo_3Sb_{12}$ that is significantly larger than in $CoSb_3$. Unfortunately, we are not aware of any experimental data to which we can compare this result. In spite of the error in its absolute value, we expect the increase of the dielectric constant to be trustable since it is reasonable to assume that the LDA error in ε_∞ is of the same magnitude in both compounds.

The increase of ε_∞ can have distinct origins. On the one hand, based on a simple Clausius–Mossotti model [44], the polarizabilities of the Tl^+ ions add to the dielectric susceptibility of

Table 3. Bader ionic charges Q_i ($|e|$) in $CoSb_3$ and $TlFeCo_3Sb_{12}$. We consider explicitly the transition metal atoms Co_1 and Co_2/Fe located respectively in $(\frac{1}{4}, \frac{1}{4}, \frac{1}{4})$ and $(-\frac{1}{4}, \frac{1}{4}, \frac{1}{4})$, the Sb atom in $(-z, 0, y)$ and the Tl atom at the origin (see section 3.1 for the definition of the atomic positions).

$CoSb_3$		$TlFeCo_3Sb_{12}$	
		Tl	0.29
Co_1	−0.53	Fe	−0.36
Co_2	−0.53	Co_2	−0.48
Sb	0.17	Sb	0.12

the unfilled compound to yield a larger ε_∞ in $TlFeCo_3Sb_{12}$. On the other hand, the increase can be due to the dielectric constant of the host crystal that is increased due to the presence of Tl and Fe in the filled compound. To check which mechanism applies in $CoSb_3$, we decomposed the optical dielectric tensor into contributions originating from the individual groups of bands of figure 1. This decomposition reveals that the deeper bands (Sb 5s, Tl 5d and Tl 6s) can only be weakly polarized by an electric field (they contribute less than 0.1% to ε_∞) and that the contribution of the Sb 5p and transition metal 3d electrons is strongly increased in the filled compound. We can therefore conclude that the increase of ε_∞ is due to a modification of the dielectric constant of the host crystal, while the polarizability of Tl^+ plays only a minor role.

4.2. Effective ionic charges

In table 3, we report the static ionic charges Q_i ($|e|$) in $CoSb_3$ and $TlFeCo_3Sb_{12}$ obtained from a topological analysis following Bader's prescription for the partitioning of space into atomic basins [17]. In this approach, one has to determine surfaces that obey the zero-flux condition for the electron density $n(\mathbf{r})$: $\nabla n \cdot \boldsymbol{N} = 0$, where $\boldsymbol{N}$ is the vector normal to the surfaces. The integration of $n(\mathbf{r})$ within each atomic basin yields the ionic charge Q_i of the related atom i.

In both compounds the chemical bonds have a negligible ionic character, as is revealed by the small Q_i. In contrast to these small static charges, the dynamical Born effective charges $Z^*_{\kappa,\alpha\beta}$ (the index κ labels an atom in the unit cell and α, β are two Cartesian directions) shown in table 4 are very large. They are comparable to the giant effective charges in ferroelectric ABO_3 compounds [45] as well as in other narrow band gap semiconductors such as Al_2Ru [41]. In the ferroelectrics, the amplitude of the $Z^*_{\kappa,\alpha\beta}$ can be explained thanks to the Harrison model [46]: a relative displacement of B and O atoms generates a giant dipole moment due to a dynamical change of hybridization between O 2p and B d atomic orbitals [47]. In $CoSb_3$, the highest valence bands result from hybridizations between Co 3d and Sb 5p atomic orbitals [30]. Moreover, the structure of this compound is formed of distorted $CoSb_6$ octahedra similar to the BO_6 octahedra of the ABO_3 ferroelectrics. It is reasonable to assume that a similar mechanism takes place in $CoSb_3$ and that the large effective charges are generated by dynamical changes of hybridizations between Co 3d and Sb 5p atomic orbitals.

In skutterudites, giant effective charges have been measured from infrared spectroscopy for UFe_4P_{12} ($|Z^*_{Fe}| = 8.9|e|$) and $CeFe_4P_{12}$ ($|Z^*_{Fe}| = 11|e|$) [43]. In $CoSb_3$, we obtain[2] a value of $6.04|e|$ for $|Z^*_{Co}|$ from the amplitude of the LO–TO splitting reported in [48] and the optical dielectric constant of [39]. This value is in good agreement with that reported in table 4.

In the filled compound, the effective charge of Tl is also highly anomalous. It is significantly larger than its static ionic charge reported in table 3. Moreover, it is larger than its

[2] In [48], Lutz and Kliche report a value of 3.93 for $|Z^*_{Co}|$. However, they used a value of 10.84 for the optical dielectric constant to deduce $|Z^*_{Co}|$ from the LO–TO splitting of the infrared active phonons. This value was corrected to 25.6 in a later work [39].

Table 4. Born effective charges ($|e|$) in $CoSb_3$ and $TlFeCo_3Sb_{12}$. We consider explicitly the transition metal atoms Co_1 and Co_2/Fe located respectively in $(\frac{1}{4}, \frac{1}{4}, \frac{1}{4})$ and $(-\frac{1}{4}, \frac{1}{4}, \frac{1}{4})$, the Sb atom in $(-z, 0, y)$ and the Tl atom at the origin (see section 3.1 for the definition of the atomic positions).

	$CoSb_3$				$TlFeCo_3Sb_{12}$		
				Tl	3.64	−0.05	−0.02
					−0.02	3.64	−0.05
					−0.05	−0.02	3.64
Co_1	−6.89	0.82	0.34	Fe	−9.83	1.13	−0.20
	0.34	−6.89	0.82		−0.20	−9.83	1.13
	0.82	0.34	−6.89		1.13	−0.20	−9.83
Co_2	−6.89	−0.82	−0.34	Co_2	−7.28	−0.75	0.08
	−0.34	−6.89	0.82		−0.09	−7.30	0.73
	−0.82	0.34	−6.89		−0.64	−0.10	−7.34
Sb	2.63	0.00	0.42	Sb	2.43	−0.10	−0.04
	0.00	1.94	0.00		−0.03	1.87	0.01
	0.68	0.00	2.32		1.01	0.12	2.13

nominal ionic charge of $+1|e|$ that would be expected if there was a complete transfer of the 6p electron to the atoms of the cage.

The effective charges of Co and Sb being similar in the filled and the unfilled compounds, the effective charge introduced by Tl cannot be compensated by these two atoms in order to satisfy the charge neutrality condition [20] $\sum_\kappa Z^*_{\kappa,\alpha\beta} = 0$. As can be seen in table 4, $|Z^*_{Fe}|$ is about $3|e|$ larger than the absolute value of the effective charge of the Co atom that it substitutes. As mentioned in section 3.1, the 6p electron of Tl is compensated by a hole in the 3d orbitals of Fe. In the case of the Born effective charges, Fe plays a similar role: due to the fact that $|Z^*_{Fe}|$ is larger than $|Z^*_{Co}|$, the anomalous effective charge of Tl is mainly compensated by the anomalous effective charge of Fe. A plausible mechanism for this compensation is that the Tl 6p electron is partially shared between Tl and Fe, so it might be responsible for a transfer of charge during a relative displacement of these two atoms.

5. Zone-centre phonons

5.1. Potential energy

To understand the effect of Tl filling on the lattice thermal conductivity of $CoSb_3$, it is mandatory to investigate the dynamics of these atoms in their cages. Experimentally, unusually large atomic displacement parameters (ADPs) have been observed for various filling atoms [3, 35]. To decide whether these ADPs are due to quasi-harmonic vibrations about the centre of the cage or to the random hopping between off-centre sites [37], it is important to investigate the shape of the potential energy well.

To that end, we computed the variations of the total energy for a rigid displacement of the Tl sublattice along various directions, keeping constant the positions of all other atoms. Figure 3 shows the results for the crystallographic [1 0 0] direction. We see that the centre of the cage is the global minimum of the potential energy well and not a saddle point as has been suggested previously [37]. Close to the origin, the energy changes quadratically with the atomic positions (dashed line). The whole energy region of figure 3 can be fitted accurately by

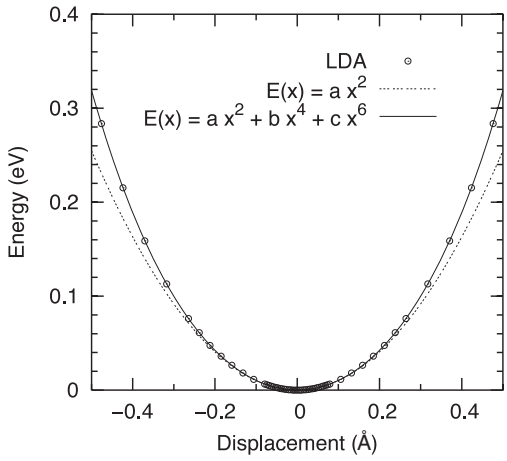

Figure 3. Potential energy associated to a cooperative displacement of Tl along [1 0 0].

a sixth-order polynomial (full line). The related harmonic frequency is 52 cm^{-1}. This so-called 'bare frequency' is quite independent of the direction of the atomic displacement: for the [1 1 0] and [1 1 1] directions, we obtained values that differ by less than 0.3 cm^{-1} from the one of figure 3. In case of Tl, the bare frequency is smaller than that of Ce (68 cm^{-1}) and La (74 cm^{-1}) in $CeFe_4Sb_{12}$ and $LaFe_4Sb_{12}$ [6]. This result is surprising. On the basis of the crystal radii [49] of Tl^{1+} (1.84 Å), Ce^{3+} (1.48 Å) and La^{3+} (1.50 Å) in a 12-coordinate site we could expect the repulsion between ionic cores to be more important between Tl and Sb than between Ce/La and Sb. The energy should therefore increase more rapidly for an off-centre displacement of Tl and the curvature of the potential energy well should be stronger. However, in section 3.2 we saw that there is a significant covalent interaction between Tl and Sb. The simple argument of the crystal radii can therefore not be applied in case of $TlFeCo_3Sb_{12}$ because the atoms do not behave like rigid spheres.

The large ADPs of Tl have been attributed to an Einstein oscillator [3] with an eigenfrequency of 36 cm^{-1}. This value is close to the Einstein frequencies deduced from specific heat measurements and inelastic neutron scattering experiments [9] (39 ± 1 cm^{-1}) but it is significantly lower than the computed Tl bare frequency. This difference between the bare frequency and the normal mode frequency observed experimentally will be further discussed in section 5.2.

5.2. Normal mode frequencies

The unfilled skutterudite $CoSb_3$ belongs to the space group $Im\bar{3}$. At the Γ-point, the zone centre optical phonons can be classified according to its irreducible representations

$$2A_g + 2E_g + 4F_g + 2A_u + 2E_u + 7F_u. \quad (1)$$

Only the F_u-modes are infrared active. At the Γ-point, they are split into transverse (TO) and longitudinal (LO) modes. Only the A_g, E_g and F_g are Raman active.

In table 5, we report the frequencies (cm^{-1}) of the TO and LO modes in $CoSb_3$ and $TlFeCo_3Sb_{12}$. The values in the unfilled compound are compared to the first-principles and force-constant (FC) model calculations of Feldman and Singh (model A of [26]) and to the experimental data obtained by infrared [48] and Raman [50] spectroscopy. The overall agreement between theory and experiment is good. In particular, the phonon frequencies in

Table 5. Frequencies (cm^{-1}) of the transverse and longitudinal zone-centre optical phonons in $CoSb_3$ and $TlFeCo_3Sb_{12}$. The phonons in the unfilled compound are classified according to the irreducible representations of the space group $Im\bar{3}$. LM denotes the Tl-dominated local modes in $TlFeCo_3Sb_{12}$. The other phonons in $TlFeCo_3Sb_{12}$ are associated to the mode of the unfilled compound with whom the overlap is the strongest. In case the degeneracy of a mode is lifted in the filled compound, we report the frequencies of all resulting phonons. The first and second values in column 6 are respectively one and two times degenerated. The values of [7] in the two last columns were obtained for $LaFe_4Sb_{12}$, for which the lattice dynamics is expected to be similar to that of $TlFeCo_3Sb_{12}$.

	Unfilled				Filled		
Mode	LDA[a]	LDA[b]	FC[b]	Exp.	LDA[a]	LDA[f]	Exp.
LM^T					41, 42	54	40[e]
LM^L					45		
A_g	141	150	151	135[c]	145	148	147[f]
	169	179	177	186[c]	155	156	154[f]
A_u	116	109	110		112	92	
	236	241	240		224	212	
E_g	122		139		123	133	122[f]
	175		183		157	158	161[f]
E_u	133		131		130	125	
	246		267		228	251	
F_g	87		83	82[c]	93, 92	95	94[f]
	105		97	109[c]	98, 101	101	102[f]
	143		157	152[c]	133, 136	137	131[f]
	173		178	178[c]	166, 163	164	172[f]
F_u^T	80		78	78[d]	85	94	
	117		120	120[d]	116	119	
	136		144	144[d]	137, 135	140	
	167		175	174[d]	152	151	
	232		241	247[d]	217, 215	223	
	245		261	257[d]	248, 233	241	
	258		277	275[d]	238, 261	259	
F_u^L	80			81[d]	85		
	119			124[d]	118		
	137			147[d]	137, 135		
	168				152		
	244			252[d]	233, 230		
	250			262[d]	244, 241		
	273			288[d]	267, 274		

[a] Present: $CoSb_3$ and $TlFeCo_3Sb_{12}$.
[b] LDA and force-constant (FC) model calculations [26] for $CoSb_3$.
[c] Raman spectroscopy [50] for $CoSb_3$.
[d] Infrared spectroscopy [48] for $CoSb_3$.
[e] Inelastic neutron scattering [9] for $TlCo_4Sb_{12}$.
[f] LDA + Raman data on $LaFe_4Sb_{12}$ [7].

the low-energy region—the region of the Tl vibrations in the filled compound—are accurately reproduced.

We should note that the Raman measurements of [50] were performed on polycrystalline samples. As a consequence, only the A_g modes were identified in this study, while the remaining Raman lines can be either associated to E_g or F_g modes. In table 5, we identify four

of the additional frequencies to the theoretical F_g modes. In fact, the experimental frequencies of 82, 109 and 152 cm^{-1} are close to the three lowest F_g modes obtained in our study and by Feldman and Singh [26]. In the case of the mode at 178 cm^{-1}, this identification is less clear since its frequency is close to the highest E_g mode and the highest F_g mode. In addition to these four modes, the authors of [50] report a mode at 60 cm^{-1} (not reported in table 5) that is not confirmed by our calculation or by the calculation of Feldman and Singh [26]. Therefore, we do not associate this Raman line to a phonon mode in $CoSb_3$.

In spite of the giant effective charges, the transverse and longitudinal F_u modes are rather close in energy. Such a small amplitude of the LO–TO splitting can be attributed to the large optical dielectric constant (see section 4.1) that screens the macroscopic electric field generated by the longitudinal polar lattice vibrations. At lower energies, this screening is almost perfect and the LO and TO modes are nearly degenerate. At higher energies, we observe a small increase in the frequency of the LO modes with respect to the TO modes. We will see in the next section that vibrations of Co and Sb respectively dominate the low- and high-energy regions. The larger amplitude of the LO–TO splitting at higher energies can therefore be attributed to the giant effective charges of Co that are about three times larger than those of Sb.

In $TlFeCo_3Sb_{12}$, the presence of Fe breaks the symmetry of the crystal lattice. Consequently, it is no longer possible to classify the phonon modes according to equation (1). Nevertheless, the eigenvectors of most phonons are only slightly modified. From the overlap between eigenvectors in the filled and unfilled compounds, it is possible to associate each phonon in $TlFeCo_3Sb_{12}$ to a mode in $CoSb_3$. Due to the symmetry breaking, the degeneracy of some phonons is lifted in $TlFeCo_3Sb_{12}$. In this case, we report the frequencies of all the resulting modes if they differ by more than 1 cm^{-1}. The first and second values in the last column of table 5 are respectively one and two times degenerated.

The TO modes in $TlFeCo_3Sb_{12}$ that have the strongest overlap with the F_u^T modes of the unfilled compound are polar. The frequencies of the corresponding LO modes are reported at the end of table 5. In addition, other modes become polar in the filled compound. Among them, the highest A_u and E_u modes acquire the strongest polarity. Nevertheless, the splitting between the corresponding TO and LO modes is rather weak and is not reported in table 5.

At 40 cm^{-1}, we observe three additional polar modes in the filled compound. Experimentally, a peak in the phonon density of states of $TlFeCo_3Sb_{12}$ has been observed at this frequency [9]. This peak has been attributed to a localized vibration of Tl in its cage. Our calculation confirms the strong contribution of Tl to these modes. About 88% of the eigenvectors are due to the vibrations of Tl. The frequencies of these modes are significantly smaller than the bare frequency of a pure (100%) Tl vibration reported in section 5.1 (52 cm^{-1}). This difference between the bare frequency and the frequency of the local Tl mode (LM) can be attributed to hybridizations between the pure Tl vibrations and the phonons of the unfilled compound.

To the authors' knowledge, no experimental data on the zone-centre phonons of $TlFeCo_3Sb_{12}$ are available. However, in a recent work, Feldman and co-workers [7] measured the frequencies of the Raman-active modes in $La_{0.75}Fe_3CoSb_{12}$. In addition, they used first-principles calculations to compute the frequencies of all zone-centre optical phonons in $LaFe_4Sb_{12}$. The results of their studies are reported in table 5, where they are compared to our theoretical results for $TlFeCo_3Sb_{12}$, although they were obtained for a different compound.

The Raman-active modes are dominated by the dynamics of Sb. In section 6, we will see that the vibrations of Sb are almost decoupled from those of Co/Fe. We can therefore expect the frequencies of the Raman active modes to be similar in $TlFeCo_3Sb_{12}$ and the La-filled skutterudites. In table 5, we see that this is indeed the case and that the agreement between our results and those of Feldman and co-workers is quite good for most of the Sb-dominated

Table 6. Electronic and ionic contributions of individual phonon modes to the static dielectric constant in $CoSb_3$ and $TlFeCo_3Sb_{12}$. LM denotes the Tl-dominated local modes in $TlFeCo_3Sb_{12}$.

	$CoSb_3$		$TlFeCo_3Sb_{12}$	
	ω_m (cm^{-1})	ε_0	ω_m (cm^{-1})	ε_0
ε_∞		31.67		38.57
LM			41, 42	10.77
F_u	80	0.09	85	0.07
A_u			112	0.00
F_u	117	1.76	116	2.00
E_u			130	0.02
F_u	136	0.38	137, 135	0.23
F_u	167	0.09	152	0.13
F_u	232	6.44	217, 215	8.04
A_u			224	0.93
E_u			228	0.06
F_u	245	0.49	248, 233	0.94
F_u	258	1.52	238, 261	2.07
Total		42.44		63.83

modes between 80 and 200 cm^{-1}. The frequency of the La-dominated mode in $LaFe_4Sb_{12}$ is larger than that of the Tl-dominated mode in $TlFeCo_3Sb_{12}$. This result will be discussed more in detail in section 6.

5.3. Infrared reflectivity and static dielectric tensor

The static dielectric constant ε_0 can be decomposed into an electronic and an ionic part [51]:

$$\varepsilon_0 = \varepsilon_\infty + \sum_m \Delta\varepsilon_m. \tag{2}$$

$\Delta\varepsilon_m$ represents the contribution of zone-centre TO mode m and can be computed from the infrared oscillator strength S_m, the phonon frequency ω_m and the unit cell volume Ω_0

$$\Delta\varepsilon_m = \frac{4\pi}{\Omega_0}\frac{S_m}{\omega_m^2}. \tag{3}$$

In table 6, we report the decomposition of ε_0 for both $CoSb_3$ and $TlFeCo_3Sb_{12}$.

In the unfilled compound, the ionic contribution is dominated by the F_u mode at 232 cm^{-1} that has the strongest oscillator strength ($S_m = 14.29 \times 10^{-4}$ au). Such a large oscillator strength can be compared to the oscillator strengths of the high polar modes in ferroelectric oxides such as $LiNbO_3$ [52]. In addition, the frequency of this mode is of the same magnitude as the frequency of the most polar modes in $LiNbO_3$. However, $\Delta\varepsilon_m$ is small compared to the ionic contribution to ε_0 in ferroelectrics. This surprising result is due to the fact that $CoSb_3$ has a relatively open structure characterized by a large unit cell volume. In $CoSb_3$, the primitive unit cell contains 16 atoms and has a volume $\Omega_0 = 369.20$ Å^3 that is more than three times larger than the volume of the ten-atom unit cell in $LiNbO_3$ ($\Omega_0 = 101.70$ Å^3).

In $TlFeCo_3Sb_{12}$, the static dielectric tensor is no longer isotropic but presents weak off-diagonal elements. As for the optical dielectric tensor, these elements are about two orders of magnitude smaller than the diagonal ones. To a good approximation, we can therefore neglect them and characterize the dielectric tensor by its single diagonal element ε_0. The decomposition of ε_0 in the filled compound is more complicated than in the unfilled. The values reported for

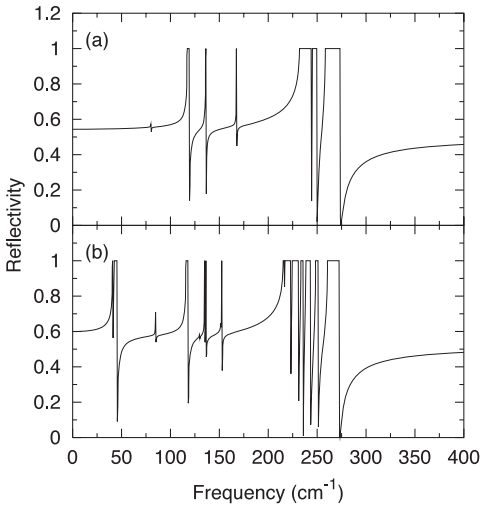

Figure 4. Infrared reflectivity of $CoSb_3$ (a) and $TlFeCo_3Sb_{12}$ (b).

the F_u modes in table 6 correspond to the sum of the $\Delta\varepsilon_m$ of the three modes that have been split in the filled compound (see section 5.2).

In $TlFeCo_3Sb_{12}$, ε_0 is about 50% larger than in $CoSb_3$. Part of this increase can be attributed to the electronic contribution that increases by 6.89, as discussed in section 4.1, and to the ionic contribution of the F_u modes that is slightly larger in the filled compound. In addition, due to its lower symmetry, the A_u and F_u modes become infrared active in the filled compound although their contribution to ε_0 is weak. The most important part (10.77) comes from the Tl-dominated mode at 42 cm^{-1}. Its oscillator strength ($S_m = 0.79 \times 10^{-4}$ au) is rather low compared to that of the Co/Fe-dominated modes at high energy. But, due to its low frequency, the contribution of this additional mode in the filled compound is very important. This result demonstrates that Tl filling has an important influence on the static dielectric constant of $CoSb_3$. It suggests that materials with a structure characterized by large empty voids might be interesting candidates for applications that require a well-defined dielectric constant since the value of ε_0 can be tuned by filling the voids (or a fraction of them) with guest atoms.

From the analysis of the results presented in this paper, we can identify some general criteria that should be satisfied by an element in order to be efficient for such a tuning of the dielectric constant. On the one hand, the Born effective charge of the filling atom should be as high as possible. This requires a certain amount of hybridization between the guest atoms and the atoms of the host crystal. On the other hand, the bare frequency of the filling atom should be as low as possible since we expect the normal mode frequency to increase with the bare frequency. In spite of the hybridization necessary for a high polarizability and Born effective charge, this second condition requires a filling atom weakly bound to ensure a low curvature of the potential energy well. In addition, the mass of the filling atom, M, must be high since the bare frequency is proportional to $1/\sqrt{M}$.

Figure 4 shows the infrared reflectivity of $CoSb_3$ (a) and $TlFeCo_3Sb_{12}$ (b) computed from the Born effective charges and phonon frequencies and eigenvectors, as is described in [51]. Since this approach neglects the damping of the phonon modes, the curves saturate to 1. For the unfilled compound, there is a qualitative good agreement between figure 4(a) and the reflectivity measured by Lutz and Kliche [39, 48]. The most striking difference between the reflectivity of $CoSb_3$ and $TlFeCo_3Sb_{12}$ is the presence of a well-defined band below 50 cm^{-1} that is related

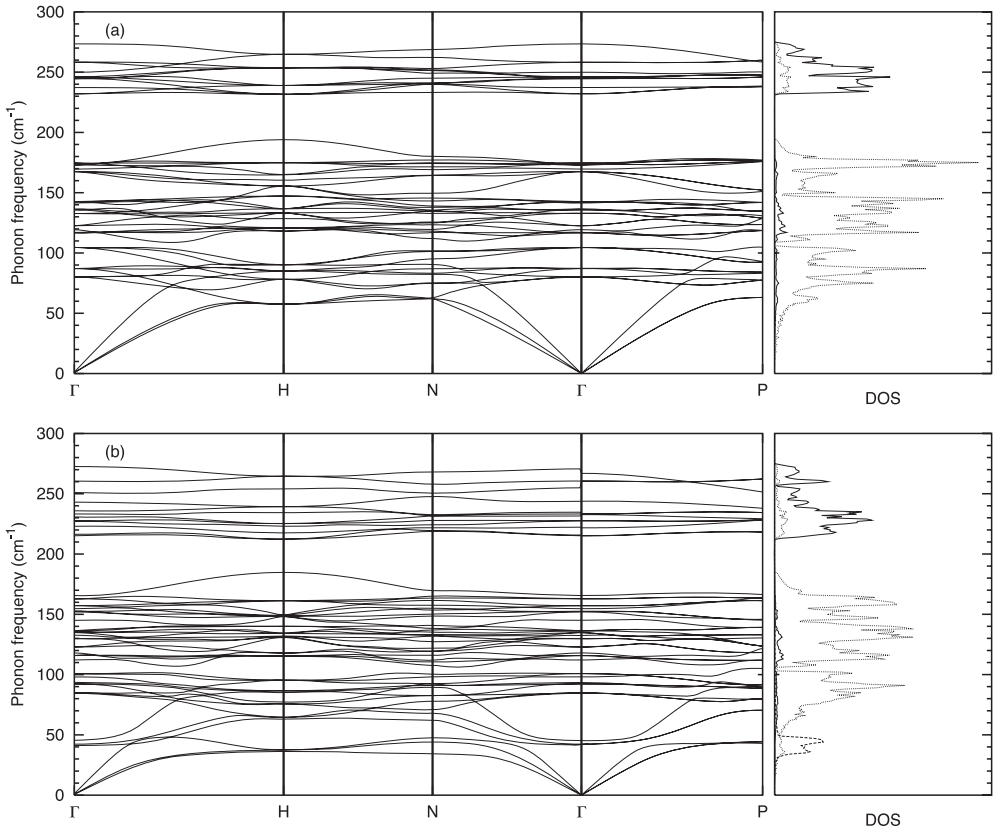

Figure 5. Phonon dispersion and projected DOS in $CoSb_3$ (a) and $TlFeCo_3Sb_{12}$ (b). The full, dashed and dotted lines in the DOS show respectively Co/Fe, Tl and Sb vibrations.

to the Tl-dominated mode and the large Tl Born effective charge (section 4.2). In addition, we observe the appearance of a few lines associated to the A_u and E_u modes that become infrared active in the filled compound as discussed above. Unfortunately, we are not aware of any experimental reflectivity measurements for $TlFeCo_3Sb_{12}$. Dordevic and co-workers [43] measured the reflectivity of MFe_4P_{12} filled skutterudites (M = La, Th, Ce, U) and observed a similar strong band associated to the M-dominated mode. This shows that infrared spectroscopy is an appropriate technique to study the dynamics of the filling atoms in skutterudites.

6. Phonon dispersion curves, density of states and specific heat

Figure 5 shows the phonon dispersion curves and projected DOS of $CoSb_3$ (a) and $TlFeCo_3Sb_{12}$ (b). In both compounds, the vibrations of Co/Fe and Sb are mainly decoupled and occupy respectively the high-energy region above 220 cm^{-1} and the low-energy region below 200 cm^{-1}.

The computed DOS of $CoSb_3$ is in good agreement with the DOS obtained from various force constant model calculations by Feldman and Singh [26]. At low frequency, the agreement is nearly perfect. All calculations also predict a large gap at about 200 cm^{-1} and a smaller gap at about 100 cm^{-1}. We do not properly reproduce the two well-defined peaks above 200 cm^{-1} reported in [26] (calculations) and [53] (experiment). This might be due to a lack of accuracy in

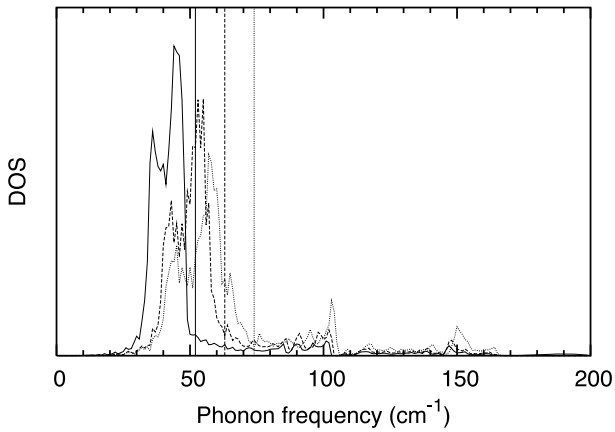

Figure 6. Tl-projected DOS in $TlFeCo_3Sb_{12}$ (full line), Tl-projected DOS obtained by artificially decreasing the mass of Tl to that of La (dashed line) and Tl-projected DOS obtained by changing both the mass and the curvature of the potential energy well to those of La (dotted line). The vertical lines indicate the positions of the corresponding bare frequencies.

our calculation of the high-energy part of the spectrum. In table 5, we see that the frequencies above 200 cm^{-1} tend to underestimate the experiment while those below 200 cm^{-1} are more accurate. The small deviations at high energy do not affect the following discussions, that focus on the lower part of the spectrum.

In the filled compound, an additional branch at about 40 cm^{-1} gives rise to a well-defined peak in the DOS that is not present in the unfilled compound. A peak at the same frequency has been observed by inelastic neutron scattering [9] in the DOS of $TlCo_4Sb_{12}$. By comparing the DOS of filled and unfilled compounds, the authors of [9] attributed this peak to a localized oscillation of Tl. As can be seen in figure 5, the peak at 40 cm^{-1} is strongly dominated by the vibrations of Tl that show only weak hybridization with Sb. This result gives therefore a strong argument in favour of the interpretation of [9].

Experimentally, a difference has been observed between the DOS of Tl- and La-filled skutterudites. The authors of [9] report the existence of a single Tl-dominated peak in $TlFeCo_3Sb_{12}$ at 40 cm^{-1} while the authors of [5] claim that there are two La-dominated peaks in the DOS of $LaFe_4Sb_{12}$ at 56 and 121 cm^{-1}. Our calculation clearly confirms the existence of a single peak in $TlFeCo_3Sb_{12}$ (solid line in figure 6). In section 5.1, we saw that the bare frequency of Tl (52 cm^{-1}) is significantly smaller than that of La (74 cm^{-1}), a difference that must be attributed to the larger Tl mass and a weaker curvature of the Tl potential energy well.

If we redo our calculations for a fictitious compound in which we artificially reduce the mass of Tl to that of La, the Tl vibrational frequency is shifted to 48 cm^{-1} and yields a marginal increase in the DOS around 100 cm^{-1} (dashed line in figure 6). Further, if we artificially strengthen the interaction of Tl with the lattice by increasing the interatomic force constants in order to fit the curvature of the potential energy well of La, the main Tl vibrational peak is shifted at 51cm^{-1} and we observe the appearance of a second peak around 100 cm^{-1}. This suggests that the peak at 121 cm^{-1} reported by Keppens and co-workers [5] cannot be attributed to an additional localized mode but rather to phonon modes that are formed by coupled Sb–La vibrations. Generally, it appears that the coupling between the La and Sb vibrations is more important than between Tl and Sb vibrations, because in the former case the bare frequency is closer to the energy region of the Sb-dominated optical phonons. This interpretation of the second peak reinforces the arguments of Feldman and co-workers in [6].

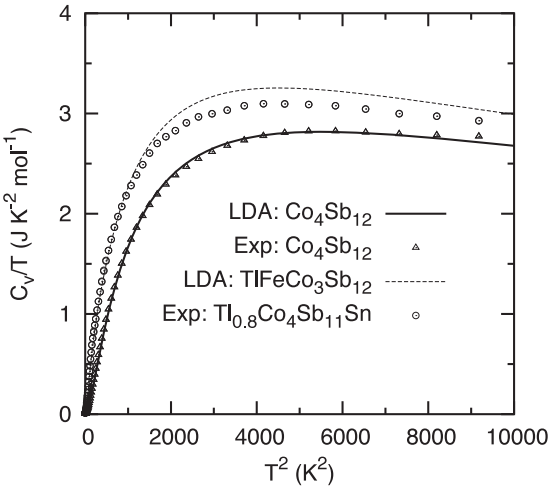

Figure 7. Theoretical and experimental heat capacity of $CoSb_3$ and Tl-filled $CoSb_3$ divided by the temperature as a function of the square of the temperature. Experimental results are from [9].

As discussed above, the vibrations of Co/Fe are located in the high-energy region of the phonon spectrum, so they are mainly decoupled from the vibrations of Tl. This result *a posteriori* justifies our approximation of neglecting the disorder due to the random substitution of one Co atom per cell by Fe (see section 2). Since the vibrations of Tl and Co/Fe are only weakly coupled, we expect the influence of such a disorder to be small. This hypothesis is further confirmed by the observation that the Tl peak in the experimental DOS [9] is broader in the Sn-compensated compound $TlCo_4Sb_{11}Sn$ than in $TlFeCo_3Sb_{12}$. In fact, the vibrations of Tl are located in the same energy region as that of Sb/Sn. As a consequence, there are significant hybridizations between the vibrations of those atoms. We expect therefore that the disorder due to the random substitution of one Sb per cell by Sn has a stronger influence on the dynamics of the filling atom than the substitution of Co by Fe.

Due to the rather flat dispersion of the optical branches, we expect the lattice thermal conductivity of $CoSb_3$ to be dominated by the acoustic phonons. As can be seen in figure 5(b), the Tl-derived modes cut through the acoustic branches. A similar effect has been observed recently in Sr-filled Ge clathrates from atomic simulations making use of empirical interatomic potentials [54]. Using molecular dynamics simulations, the authors of [54] showed that the Sr-derived modes reduce the lattice thermal conductivity of the clathrates by approximately one order of magnitude by scattering the heat-carrying acoustic phonons. This scattering is enhanced at the frequency of the Sr modes because of the resonant interaction with the acoustic phonons [55–57]. In the same way, the resonant interaction between the Tl-derived modes and the acoustic branches might have a similar strong effect on the thermal conductivity of $CoSb_3$ and be one major source of the important decrease observed experimentally [3].

Figure 7 shows the heat capacity at constant volume of $CoSb_3$ and $TlFeCo_3Sb_{12}$ computed by integrating the phonon DOS as described in [25]. Our results are compared to the experimental values of [9] measured for $CoSb_3$ and $Tl_{0.8}Co_4Sb_{11}Sn$ at constant pressure. For the unfilled compound, the agreement between theory and experiment is excellent. In the filled compound, we observe a slight deviation from the experimental data. Part of the discrepancy can probably be attributed to the fact that the experiment was performed on a Sn-compensated sample with only partial void filling. In particular, the substitution of Sb by Sn is likely to have

a stronger effect on the specific heat at low temperatures than the substitution of Co by Fe since the Sb/Sn vibrations are at lower energy than that of Co/Fe.

7. Conclusions

In this work, we performed first-principles DFT calculations of the electronic, dielectric and dynamical properties of $CoSb_3$ and $TlFeCo_3Sb_{12}$.

Because of hybridizations between Tl and Sb, the Tl 6s electrons are partially delocalized on the Sb atoms. This result is consistent with the fact that Tl can be inserted into the voids of $CoSb_3$ in spite of its large ionic radius.

The electronic dielectric constants of $CoSb_3$ and $TlFeCo_3Sb_{12}$ are quite large, with a significantly larger value in the filled compound. This increase cannot be explained in the framework of a Clausius–Mossotti model where the Tl^+ polarizability is supposed to add to the dielectric constant of $CoSb_3$. Instead, it is the dielectric constant of the host crystal that is increased upon Tl filling accompanied by a substitution of one Co atom per cell by Fe.

Due to the negligible ionic character of the chemical bonds in $CoSb_3$ and $TlFeCo_3Sb_{12}$, the *static* atomic charges of both compounds are rather small. In contrast, the *dynamic* Born effective charges are found to be anomalously large, and of the same order of magnitude as in ferroelectric oxides.

The change in energy under a rigid displacement of the Tl sublattice revealed that the centre of the cage is the global minimum of the potential energy and not a saddle point as has been suggested previously. In the filled compound, the presence of Tl gives rise to a *single* peak in the phonon DOS. Due to the hybridizations between the vibrations of Tl and Sb, this peak is significantly lower in frequency than the Tl bare frequency computed from the curvature of the potential energy well. However, these hybridizations are modest compared to those of the La-filled skutterudites, where they give rise to a second La peak in the DOS.

The Tl-dominated mode at the Γ-point is polar and gives rise to a well-defined band in the infrared reflectivity spectrum at low frequency and a strong increase of the static dielectric constant in the filled compound. On the one hand, this result shows that infrared spectroscopy can act as a sensitive probe to study the lattice dynamics of the filling atom in skutterudites and related compounds such as clathrates. On the other hand, it suggests that the dielectric constant of materials characterized by an open structure containing empty voids can be tuned by filling the voids with guest atoms.

Acknowledgments

The authors are grateful to R P Hermann, F Grandjean, G J Long and J P Issi for helpful discussions. MV acknowledges financial support from the FNRS Belgium. This work was supported by the Volkswagen-Stiftung within the project 'Nano-sized ferroelectric Hybrids' (I/77 737), the Région Wallonne (Nomade, project 115012), FNRS-Belgium through grants 9.4539.00 and 2.4562.03, and the European Commission through the FAME Network of Excellence (Functional Advanced Materials and Engineering of Hybrids and Ceramics).

References

[1] Uher C 2001 *Semicond. Semimet.* **69** 139
[2] Sales B C, Mandrus D and Williams R K 1996 *Science* **272** 1325
[3] Sales B C, Chakoumakos B C and Mandrus D 2000 *Phys. Rev.* B **61** 2475
[4] Wood C 1988 *Rep. Prog. Phys.* **51** 459
[5] Keppens V, Mandrus D, Sales B C, Chakoumakos B C, Dai P, Coldea R, Maple M B, Gajewski D A, Freeman E J and Bennington S 1998 *Nature* **395** 876

[6] Feldman J L, Singh D J, Mazin I I, Mandrus D and Sales B C 2000 *Phys. Rev.* B **61** R9209
[7] Feldman J L, Singh D J, Kendziora C, Mandrus D and Sales B C 2003 *Phys. Rev.* B **68** 94301
[8] Nordström L and Singh D J 1996 *Phys. Rev.* B **53** 1103
[9] Hermann R P, Jin R, Schweika W, Grandjean F, Mandrus D, Sales B C and Long G J 2003 *Phys. Rev. Lett.* **90** 135505
[10] Hohenberg P and Kohn W 1964 *Phys. Rev.* **136** B864
[11] Kohn W and Sham L J 1965 *Phys. Rev.* **140** A1133
[12] Gonze X, Beuken J-M, Caracas R, Detraux F, Fuchs M, Rignanese G-M, Sindic L, Verstraete M, Zerah G, Jollet F, Torrent M, Roy A, Mikami M, Ghosez Ph, Raty J-Y and Allan D C 2002 *Comput. Mater. Sci.* **25** 478 URL: www.abinit.org
[13] Perdew J P and Wang Y 1992 *Phys. Rev.* B **45** 13244
[14] Fuchs M and Scheffler M 1999 *Comput. Phys. Commun.* **119** 67
[15] Troullier N and Martins J L 1991 *Phys. Rev.* B **43** 1993
[16] Hamann D R 1989 *Phys. Rev.* B **40** 2980
[17] Bader R F W 1990 *Atoms in Molecules: A Quantum Theory* (Oxford: Oxford University Press)
[18] Casek P, Bouette-Russo S, Finocchi F and Noguera C 2004 *Phys. Rev.* B **69** 85411
[19] Monkhorst H J and Pack J D 1976 *Phys. Rev.* B **13** 5188
[20] Gonze X and Lee C 1997 *Phys. Rev.* B **55** 10355
[21] Gonze X 1997 *Phys. Rev.* B **55** 10337
[22] Veithen M, Gonze X and Ghosez Ph 2002 *Phys. Rev.* B **66** 235113
[23] Ghosez Ph and Gonze X 2000 *J. Phys.: Condens. Matter* **12** 9179
[24] Gonze X, Charlier J C, Allan D C and Teter M P 1994 *Phys. Rev.* B **50** 13035
[25] Lee C and Gonze X 1995 *Phys. Rev.* B **51** 8610
[26] Feldman J L and Singh D J 1996 *Phys. Rev.* B **53** 6273
[27] Schmidt Th, Kliche G and Lutz H D 1987 *Acta Crystallogr.* C **43** 1678
[28] Sofo J O and Mahan G D 1998 *Phys. Rev.* B **58** 15620
[29] Singh D J and Pickett W E 1994 *Phys. Rev.* B **50** 11235
[30] Lefebvre-Devos I, Lassalle M, Wallart X, Olivier-Fourcade J, Monconduit L and Jumas J C 2001 *Phys. Rev.* B **63** 125110
[31] Kurmaev E Z, Moewes A, Shein I R, Finkelstein L D, Ivanovskii A L and Anno H 2004 *J. Phys.: Condens. Matter* **16** 979
[32] Caillat T, Borshchevsky A and Fleurial J-P 1996 *J. Appl. Phys.* **80** 4442
[33] Arushanov E, Respaud M, Rakoto H, Broto J M and Caillat T 2000 *Phys. Rev.* B **61** 4672
[34] Nagao J, Ferhat M, Anno H, Matsubara K, Hatta E and Mukasa K 2000 *Appl. Phys. Lett.* **76** 3436
[35] Sales B C, Mandrus D, Chakoumakos B C, Keppens V and Thompson J R 1997 *Phys. Rev.* B **56** 15081
[36] Resta R 2002 *J. Phys.: Condens. Matter* **14** R625
[37] Nolas G S, Slack G A, Morelli D T, Tritt T M and Ehrlich A C 1996 *J. Appl. Phys.* **79** 4002
[38] Kokalj A 1999 *J. Mol. Graphics Modelling* **17** 176 URL: www.xcrysden.org
[39] Kliche G and Lutz H D 1984 *Infrared Phys.* **24** 171
[40] Gonze X, Ghosez Ph and Godby R W 1995 *Phys. Rev. Lett.* **74** 4035
[41] Öğüt S and Rabe K M 1996 *Phys. Rev.* B **54** R8297
[42] Kliche G and Bauhofer W 1988 *J. Phys. Chem. Solids* **49** 267
[43] Dordevic S V, Dilley N R, Bauer E D, Basov D N, Maple M B and Degiorgi L 1999 *Phys. Rev.* B **60** 11321
[44] Kittel C 1996 *Introduction to Solid State Physics* (New York: Wiley)
[45] Zhong W, King-Smith R D and Vanderbilt D 1994 *Phys. Rev. Lett.* **72** 3618
[46] Harrison W A 1980 *Electronic Structure and the Properties of Solids* (San Francisco, CA: Freeman)
[47] Ghosez Ph, Michenaud J-P and Gonze X 1998 *Phys. Rev.* B **58** 6224
[48] Lutz H D and Kliche G 1982 *Phys. Status Solidi* b **112** 549
[49] Shannon R D 1976 *Acta Crystallogr.* A **32** 751
[50] Nolas G S and Kendziora C A 1999 *Phys. Rev.* B **59** 6189
[51] Gonze X and Lee C 1997 *Phys. Rev.* B **55** 10355
[52] Veithen M and Ghosez Ph 2002 *Phys. Rev.* B **65** 214302
[53] Hermann R P, private communication
[54] Dong J, Sankey O F and Myles C W 2001 *Phys. Rev. Lett.* **86** 2361
[55] Pohl R O 1962 *Phys. Rev. Lett.* **8** 481
[56] Nolas G S, Weakley T J R, Cohn J L and Sharma R 2000 *Phys. Rev.* B **61** 3845
[57] Cohn J L, Nolas G S, Fessatidis V, Metcalf T H and Slack G A 1999 *Phys. Rev. Lett.* **82** 779
[58] Grandjean F, Long G J, Cortes R, Morelli D T and Meisner G P 2000 *Phys. Rev.* B **62** 12569